Challenging Glass 6 - Conference on Architectural and Structural Applications of Glass
Louter, Bos, Belis, Veer, Nijsse (Eds.), Delft University of Technology, May 2018.

ISBN 978-94-6366-044-0, https://doi.org/10.7480/cgc.6.2170

Effect of Interlayer Mechanical Properties on Quasi-static and Free Vibration Response of Laminated Glass

Alena Zemanová, Tomáš Janda, Jan Zeman, Jaroslav Schmidt, Michal Šejnoha
Czech Technical University in Prague, Czech Republic, e-mail (alena.zemanova@fsv.cvut.cz)

Laminated glass fulfills the demands on safety and security in transparent structural elements used in architecture and other fields of engineering. It can be constructed as forced-entry, bullet, or blast resistant. The basic three-layer configuration consists of two glass panes connected with a polymer or ionomer interlayer; the advanced products contain also other layers. The foil ensures shear coupling and provides post-breakage resistance and damping. For the design of laminated glass structures and their analysis, knowledge of mechanical properties of interlayers is essential. In numerical simulations, the interlayer is most typically described by the generalized Maxwell chain – a classical viscoelastic model which can capture the time/temperature-dependent response of polymers under shear. Its parameters can be found for common interlayer types in the literature. However, they differ even for the same material, because of a slightly different content of additives, different test setups, and different data processing procedures. In this contribution, the dependence of the response of a laminated glass element on the material parameters of the polymer interlayer is studied by means of numerical modelling and experiments. Two examples are shown and discussed, i.e., quasi-static analysis of a simply-supported beam and modal analysis of a free-free beam. Numerical predictions are obtained by a layer-wise model based on the finite element method. These predictions are validated against the detailed experimental data. We demonstrate that using the Maxwell model parameters from the literature determined even for the same material type but not for the concrete foil may lead to unrealistic predictions.

Keywords: Laminated Glass, Polymer, Generalized Maxwell Chain, Quasi-static Analysis, Free Vibrations

1. Introduction

Laminated glass has great potential as a transparent composite material for load-bearing and fail-safe structural elements. In its basic configuration, a three-layer composite consists of two glass layers connected with an interlayer, typically made of polymer or ionomer. This basic layout can be repeated or complemented with layers from different materials, such as polyurethane, polycarbonate, or others, to improve the post-breakage resistance or to increase the impact resistance of the element.

For numerical prediction of the response of laminated glass, knowledge of the mechanical properties of individual layers is essential. The interlayer affects the behavior and response of laminated glass significantly because it provides shear coupling, damping, and post-breakage resistance. The mechanical properties which can be found in the literature differ in some cases even for the same material. The reason of this discrepancy can be a slightly different content of additives, different test setups, and different data processing procedures.

The aim of this contribution is to study the dependence of the response of laminated glass elements on the material parameters of the polymer interlayer which were taken from the literature. These parameters for two selected polymers are presented together with the brief introduction of the viscoelastic model for the interlayer in Section 2. For this purpose, two different experiments were performed, i.e., quasi-static bending tests in a vacuum chamber and modal analysis of unsupported laminated glass beams; both of them are discussed in Section 3. The numerical modelling of these examples is briefly introduced in Section 4, and the results of experimental and numerical testing are summarized in Section 5. The effects of material properties on the behavior of laminated glass elements is also discussed, and the main findings are summarized in Section 6.

2. Polymer interlayers

Because of the time/temperature (frequency/temperature) behavior of polymers, their characterization requires several parameters to be specified. Constitutive models for these polymer foils can be found in the literature starting from the linear elastic approximation for given loading conditions (Foraboschi 2007) or (Foraboschi 2012), through the hyperelastic models, e.g., Mooney-Rivlin material (Timmel et al. 2007) or (Larcher et al. 2012), or the classical viscoelastic models such as the generalized Maxwell model (Andreozzi et al. 2014) or (Mohagheghian et al. 2017), towards fractional derivative models (Renaud et al. 2011).

In this study, we focused on the generalized Maxwell model which is typically used to capture the viscoelastic behavior of polymers. The material parameters of this model can be found for a few of the interlayer foils in the literature; see Table 1.

The generalized Maxwell model is a set of a spring element and several spring-dashpot Maxwell elements which are assembled into a parallel chain model (Christensen 2013). The time dependence of the shear modulus can be represented for the time instant t by the Prony series

$$G(t) = G_\infty + \sum_{p=1}^{P} G_p \exp^{-\frac{t}{\theta_p}} = G_0 - \sum_{p=1}^{P} G_p \left(1 - \exp^{-\frac{t}{\theta_p}}\right), \tag{1}$$

with the long-term shear modulus G_∞ corresponding to the shear modulus of the elastic spring, the moduli G_p denoting the shear modulus of the p-th unit, P is the number of viscoelastic units, and $\theta_p = \eta_p / G_p$ is the relaxation time related to the viscosity η_p. The expression can also be rewritten in terms of the instantaneous shear modulus of the chain $G_0 = G_\infty + \sum_{p=1}^{P} G_p$.

In the frequency domain, the complex-valued dynamic shear modulus is expressed for the angular frequency ω as

$$G^*(\omega) = G'(\omega) + \mathrm{i}G''(\omega) = G_\infty + \sum_{p=1}^{n} G_p \frac{\theta_p^2 \omega^2}{1+\theta_p^2 \omega^2} + \mathrm{i} \sum_{p=1}^{n} G_p \frac{\theta_p \omega}{1+\theta_p^2 \omega^2}, \tag{2}$$

where the real (elastic) part of the modulus G' is called the storage modulus, the imaginary (viscous) component G'' is the loss modulus. Temperature sensitiveness of the interlayers is taken into account by a time/temperature superposition principle; more specifically by the time shifting using the Williams–Landel–Ferry equation (Williams et al. 1955).

In tested samples, two different interlayer materials were used: PolyVinyl Butyral (PVB), Trosifol BG R20, and the Ethylene-Vinyl Acetate foil (EVA), Evalam 80-120. The relaxation shear moduli and the storage and loss moduli using six different data sets taken from the literature (five for PVB and one for EVA) are plotted in Figure 1. The references, where the corresponding parameters for the generalized Maxwell model and for time-temperature shifting can be found, are summarized in Table 1. The table provides also commercial names of polymer foils, manufacturers, testing methods used for parameter identification, numbers of Prony series terms *P*, and ranges of relaxation times. Additional details on the material testing, such as the frequency and temperature range for dynamic torsion tests and dynamic mechanical analysis or the loading scenario and ambient temperatures for the tensile relaxation and creep tests, can be found in the references. As can be seen for PVB from Figure 1, the shear moduli plotted for the temperature of 25°C differ even for the same type of polymer foil. This can be attributed to different test methods and setups or to different content of additives in polymers depending on the manufacturer. Some of the experiments were performed on a pure foil, some of them on an interlayer laminated between glass plies, which could also change the properties of the polymers. For most of the Prony series listed in Table 1, no clear specification can be found regarding the range of time/frequency domain for which the chain can be used. This information is provided only in (Andreozzi et al. 2014). For the others, this range of time/frequency domain could be estimated from the smallest and largest relaxation times θ_p. In Figure 1, all the series were plotted for the same time or frequency range to show their behavior even beyond the extreme relaxation times.

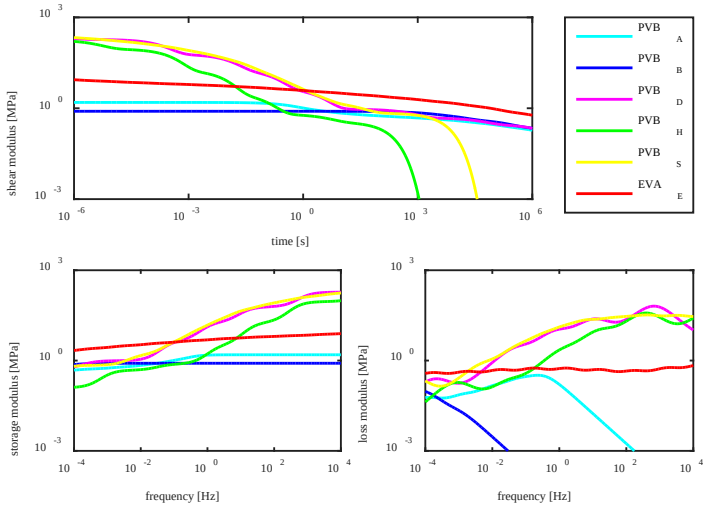

Fig. 1 Relaxation shear moduli and storage and loss shear moduli in frequency domain for PVB and EVA foils from Table 1 at 25°C.

Table 1: List of used material parameters for PVB and EVA foils with references.

Polymer	Subscript	Reference	Type/Manufacturer	Method	Prony times (range, numb.)
PVB	A	(Andreozzi et al. 2014)	Trosifol BG R20, Roberglass	Dynamic torsion test	10^{-1}–10^{7} s (10 terms)
PVB	B	(Biolzi et al. 2014)	Not known	Tens. relax. and creep test	10^{3}–10^{10} s (8 terms)
PVB	D	(Duser et al. 1999)	Butacite, DuPont	Dyn. mech. analysis	10^{-11}–10^{7} s (11 terms)
PVB	H	(Hooper et al. 2012)	Saflex PVB RB-41, Solutia	Dyn. mech. analysis	10^{-5}–10^{3} s (6 terms)
PVB	S	(Shitanoki et al. 2014)	Butacite, DuPont	Dyn. mech. analysis	10^{-7}–10^{4} s (14 terms)
EVA	E	(Eitner 2011)	Etimex Vistasolar 496.10	Dyn. mech. analysis & Tens. relax. and creep test	10^{-1}–10^{20} s (26 terms)

3. Experimental testing

Two experimental measurements were designed and performed: quasi-static analysis of a simply-supported beam and modal analysis of a free-free beam. In this section, only the setup for the quasi-static and modal analysis will be introduced. The experimental results will be discussed and compared with numerical predictions later in Section 5.

All samples were made of three-layer laminated glass. The thicknesses of glass layers were 10 mm, of the foil 0.76 mm, and the in-plane dimensions were 1,100 mm × 360 mm. The specimens were made of annealed float glass, and the PVB or EVA foil was used as the interlayer.

3.1. Quasi-static bending

The bending tests in a vacuum chamber were performed on laminated glass samples shown in Figure 1. The temperature during the experiment was 25°C. The sample was placed on two linear supports parallel to the shorter edges of the pane with soft pads made of rubber, loaded by a prescribed uniform pressure up to its collapse, and the response in terms of deflections and strains were measured according to the procedure given by (Melcher and Karmazínová 2009). The loading rate was about 0.2–0.3 kPa/s. The deflections were measured in three points on the top surface in compression, and the strain gauges were placed on six points on the top surface in compression and one at the center of the sample on the bottom surface in tension. For validation, the largest value of deflection at the center was computed from the measured value in the middle of the span from which the average of the measured deflections above the line supports was deducted. For the comparison in Section 5, the values measured along the longitudinal axis of symmetry were used. The differences in the measured values of strains at the center and near the edges were below 4%.

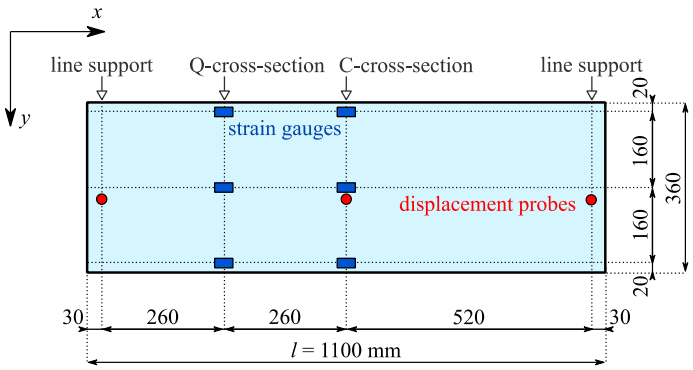

Fig. 2 Experimental setup for bending analysis of laminated glass sample.

3.2. Modal analysis

The experimental modal analysis was done to study the behavior of an unsupported laminated glass beam. For that reason, the laminated glass sample was suspended by soft strings fixed on a rigid frame as shown in Figure 3. An accelerometer was placed in the corner. The measuring device used (Brüel and Kjaer) consisted of an impact hammer type 8206, a miniature piezoelectric accelerometer type 4519-003, and a data acquisition unit type 3560-B-120. Software platforms Pulse by Brüel and Kjaer and MEscopeVES by Vibrant Technology were used for the signal acquisition and processing and for the post-processing of modal parameters.

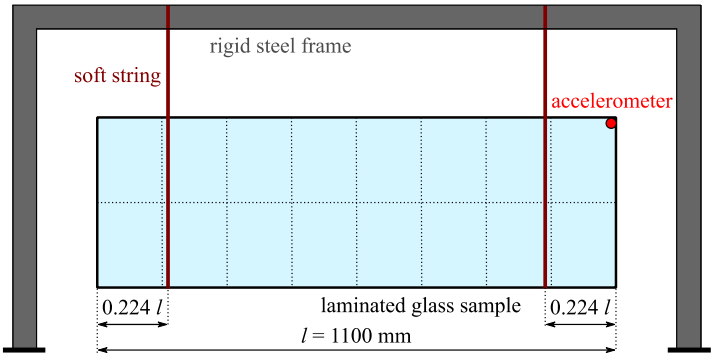

Fig. 3 Experimental setup for modal analysis of laminated glass sample.

After signal processing, the bending and torsional natural frequencies and corresponding damping ratios were extracted from the frequency response functions. The temperature during the experimental measurement was 26°C, the frequency step of the measurement was 1 Hz. The quantities corresponding to the first three bending modes are compared with our numerical predictions in Section 5. To obtain the same characteristics for damping as from the numerical analysis, the damping ratios ξ from the experimental measurement were converted to the loss factors η as follows

$$\eta \approx 2\xi. \tag{1}$$

Because the modal damping is sensitive to boundary conditions, e.g., (Zemanová et al. 2018), we attempted to assess the level of damping potentially provided by the soft hinges. For that reason, the same experiment with the setup shown in Figure 3 was performed for a monolithic glass sample with the same geometry. The measured damping ratios in this case were less than 1/20 of those for the laminated glass samples. That means that damping caused by soft hinges and by glass sheets is much smaller than that provided by the interlayer. If we neglect the effect of supports and glass layers in the numerical model, the error in damping ratios (loss factors) due to this assumption should be less than 5%.

4. Numerical analysis

In the next two sections, the quasi-static solver for bending and the eigenvalue solver for the modal analysis will be briefly introduced. For more details, the interested reader is referred to the papers by (Zemanová et al. 2017) and (Zemanová et al. 2018). Both of the developed numerical solvers, for quasi-static and modal analysis, are based on the finite element method. In the quasi-static case, the structural response is obtained using the unconditionally stable exponential algorithm. For the free vibration analysis, the structural eigenfrequencies and modal damping follow from the solution of a complex-valued nonlinear eigenvalue problem arising from the viscoelastic nature of the interlayer.

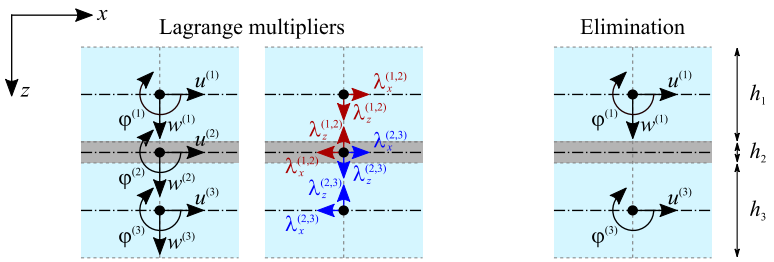

Fig. 4 Degrees of freedom per cross-section of laminated glass using Lagrange multipliers or elimination.

In both cases, a refined finite element model is used, which enables capturing the shear slip in the interlayer, and therefore the piecewise planar cross-sections after the deformation of a laminated glass sample. Every layer is taken as a shear deformable beam complemented with membrane effects, see Figure 4. This leads to three unknowns for a cross-section of a layer, i.e., two displacements and a rotation. The independent layers are connected back together using the compatibility conditions on the interfaces. Two approaches for this linking are schematically illustrated in Figure 4. On the left, the unknowns corresponding to the generalized displacement are complemented with Lagrange mutlipliers with the physical meaning of nodal forces ensuring inter-layer compatibility. This treatment increases the number of unknowns; on the other hand, the delamination phenomena could be efficiently accounted for. Additionally, a domain decomposition method for parallel computing could be employed for larger tasks. This approach was used for the quasi-static bending analysis. On the right, the dependent unknowns resulting from the inter-layer compatibility are eliminated. This approach reduces the size of the problem and was used for the modal analysis.

Linear basis functions combined with the selective integration scheme are used to avoid shear locking. From the constitutive point of view, the glass layers are treated as linear elastic, whereas the generalized Maxwell model is used to capture the viscoelastic nature of the interlayer.

4.1. Quasi-static solver for laminated glass beams

Based on the comparative study in (Zemanová et al. 2017), we employ the formulation combining the assumptions of the von Kármán kinematics for large deflections and of the constant Poisson ratio to reproduce the experimental data from Section 3.1.

The quasi-static solver is based on a few basic steps leading to the final linearized system of equations. The first is the formulation of the Lagrange function $\mathcal{L}_{n+1}$ at the time t_{n+1} in the discretized form

$$\mathcal{L}_{n+1}(\mathbf{d}, \boldsymbol{\lambda}) = \Pi_{n+1}(\mathbf{d}) + \boldsymbol{\lambda}^{\mathrm{T}}\mathbf{C}\mathbf{d}, \tag{2}$$

consisting of two parts corresponding to the total potential energy Π_{n+1} for an arbitrary kinematically admissible vector of all generalized nodal displacements $\mathbf{d}$ and to the complementary compatibility conditions, where $\boldsymbol{\lambda}$ represents the vector of admissible Lagrange multipliers and $\mathbf{C}\mathbf{d} = \mathbf{0}$ is the inter-layer compatibility, recall Figure 4. Then, the solution of the optimality conditions

$$\nabla_{\mathbf{d}}\mathcal{L}_{n+1}(\mathbf{d}_{n+1}, \boldsymbol{\lambda}_{n+1}) = \nabla\Pi_{n+1}(\mathbf{d}_{n+1}) + \mathbf{C}^{\mathrm{T}}\boldsymbol{\lambda}_{n+1} = \mathbf{0},$$

$$\nabla_{\boldsymbol{\lambda}}\mathcal{L}_{n+1}(\mathbf{d}_{n+1}, \boldsymbol{\lambda}_{n+1}) = \mathbf{C}\mathbf{d}_{n+1} = \mathbf{0}. \tag{3}$$

provides the searched nodal displacements $\mathbf{d}_{n+1}$ and Lagrange multipliers $\boldsymbol{\lambda}_{n+1}$ at time t_{n+1}.

The system is solved iteratively using the Newton method because of the geometric nonlinearity of the problem arising from the von Kármán assumptions. Thus, the $(k+1)$th approximation of $\mathbf{d}_{n+1}$ is expressed as

$${}^{k+1}\mathbf{d}_{n+1} = {}^{k}\mathbf{d}_{n+1} + {}^{k+1}\delta\mathbf{d} \text{ for } k = 0, 1 \ldots, \tag{4}$$

where the previous known iterate ${}^{k}\mathbf{d}_{n+1}$ is complemented with the increment ${}^{k+1}\delta\mathbf{d}$ determined from the linearized system

$$\begin{bmatrix} {}^{k}\mathbf{K} & \mathbf{C}^{T} \\ \mathbf{C} & \mathbf{0} \end{bmatrix} \begin{bmatrix} {}^{k+1}\delta\mathbf{d} \\ {}^{k+1}\boldsymbol{\lambda} \end{bmatrix} = - \begin{bmatrix} {}^{k}\mathbf{f}_{int} - \mathbf{f}_{ext}(t_{n+1}) \\ \mathbf{0} \end{bmatrix} \tag{5}$$

with the stiffness matrix ${}^{k}\mathbf{K}$, the matrix corresponding to the compatibility conditions $\mathbf{C}$, and the vectors of the internal and external forces ${}^{k}\mathbf{f}_{int}$ and $\mathbf{f}_{ext}(t_{n+1})$; see page 385 in (Zemanová et al. 2017).

The initial values ${}^{0}\mathbf{d}_{0}$ are set to zeros. The stopping criterion is defined as

$$\frac{\left\| {}^{k}\mathbf{f}_{int} - \mathbf{f}_{ext} + \mathbf{C}^{\mathrm{T}}\,{}^{k}\boldsymbol{\lambda} \right\|_2}{\max(\|\mathbf{f}_{ext}\|_2, 1)} < \epsilon_{\mathrm{tol}} \tag{6}$$

with the user-defined tolerance ϵ_{tol}.

4.2. Complex-valued eigensolver

Unlike in the quasi-static analysis, the real-valued shear modulus is replaced by a complex-valued dynamic shear modulus for the interlayer, and a geometrically linear formulation together with the elimination of unknowns, Figure 4, was used for the modal analysis of the task from Section 3.2. The complex-valued eigensolver is introduced in (Zemanová et al. 2018) and the main points of the derivation are summarized in this section.

In the modal analysis, a classical eigenvalue problem is formulated and complemented with a normalizing condition as follows

$$(\boldsymbol{K}(\omega) - \omega^2\boldsymbol{M})\boldsymbol{U} = \mathbf{0},$$

$$\boldsymbol{U}_0^{\mathrm{T}}(\boldsymbol{U} - \boldsymbol{U}_0) = 0, \tag{7}$$

where the mass matrix $\boldsymbol{M}$ is real-valued and constant, the stiffness matrix $\boldsymbol{K}$ is complex-valued and frequency-dependent because of the dynamic shear modulus of the interlayer, and therefore the angular natural frequency ω and the corresponding mode shape $\boldsymbol{U}$ are also complex-valued. The vector $\boldsymbol{U}_0$ corresponds to an eigenvector solving the real-valued part of the problem (7) with an initial value of shear modulus of the interlayer.

The problem from (7) is solved again iteratively using the Newton method and the linearized form of the angular natural frequency ω and the mode shape $\boldsymbol{U}$

$$
\begin{aligned}
{}^{k+1}\omega &= {}^{k}\omega + \delta\omega, \\
{}^{k+1}\boldsymbol{U} &= {}^{k}\boldsymbol{U} + \delta\boldsymbol{U}, \text{ for } k = 0, 1 \ldots,
\end{aligned}
\tag{8}
$$

compare with (4), where the $(k+1)$th approximation is determined from the previous one and the increment arising from the linearized system of equations

$$
\begin{bmatrix} \boldsymbol{K}\left({}^{k}\omega\right) - {}^{k}\omega^2\boldsymbol{M} & \left(\frac{\partial \boldsymbol{K}}{\partial \omega}\left({}^{k}\omega\right) - 2\,{}^{k}\omega\boldsymbol{M}\right){}^{k}\boldsymbol{U} \\ \boldsymbol{U}_0^{\mathrm{T}} & 0 \end{bmatrix} \begin{bmatrix} {}^{k+1}\boldsymbol{U} \\ \delta\omega \end{bmatrix} = \begin{bmatrix} \boldsymbol{0} \\ \boldsymbol{U}_0^{\mathrm{T}}\boldsymbol{U}_0 \end{bmatrix}. \tag{9}
$$

This system is solved independently for each eigenpair, i.e., the angular natural frequency and the corresponding mode shape.

The initial values are set to ${}^{0}\boldsymbol{U} = \boldsymbol{U}_0$ and ${}^{0}\omega = \omega_0$ derived from the real-valued part of the problem (7). The iterative solver is stopped when the residual drops below a given tolerance limit

$$
\frac{\left\| \left(\boldsymbol{K}\left({}^{k}\omega\right) - {}^{k}\omega^2\boldsymbol{M}\right){}^{k}\boldsymbol{U} \right\|_2}{\left\| {}^{k}\boldsymbol{U} \right\|_2} < \epsilon_{\mathrm{tol}}. \tag{10}
$$

The real-valued natural frequencies f_{Hz} and the modal factors η are extracted from the real and imaginary part of the complex-valued natural frequencies according to the following relationship

$$
\omega^2 = (2\pi f_{\mathrm{Hz}})^2(1 + \mathrm{i}\eta). \tag{11}
$$

5. Validation and discussion of results

The predictions of the measured quantities using the developed finite element solvers were validated against the experimental data. The tolerance ϵ_{tol} was set to 10^{-5}, and each layer of the laminated glass was discretized by 300 elements. Based on the experiences from our previous studies in (Zemanová et al. 2017) and (Zemanová et al. 2018), the discretization errors should be safely below 1% for all quantities presented later.

The material parameters of the generalized Maxwell model were taken from (Andreozzi et al. 2014), (Biolzi et al. 2014), (Duser et al. 1999), (Hooper et al. 2012), (Shitanoki et al. 2014), and (Eitner 2011). The Poisson ratio of interlayers was set to 0.49 and the density of PVB to 1,100 kg/m^3 and EVA to 950 kg/m^3. For glass, the density was assumed 2,500 kg/m^3, the Poisson ratio was set to 0.22, and the Young modulus of the value 76.6 GPa was measured by indentation technique. The same values were used for the quasi-static and modal analyses.

5.1. Deflections and strains from quasi-static analysis

For the quasi-static analysis of laminated glass samples from Section 3.1, the loading scenarios for both interlayers are shown in Figure 5 together with the measured and predicted response of the sample in terms of the deflection and the largest value of the tensile strain at the center of the specimen. The loading rate was about 0.3 kPa/s for the PVB sample and 0.2 kPa/s for the EVA sample. The collapse occurred at the loading time 82 s and pressure 17 kPa for the PVB sample and 134 s and 29 kPa for the EVA sample.

For PVB interlayers, the best agreement of the numerical prediction with the measured response can be seen from Figure 5 for material parameters from (Duser et al. 1999). On the other hand, the values of deflections and stains are significantly overestimated for the parameters from (Hooper et al. 2012). An excellent agreement was found between the experimental data for the EVA sample and its numerical prediction using the data from (Eitner 2011).

Table 2: Quasi-static analysis: Comparison of experimental data and numerical predictions corresponding to the largest loading pressure.

Data	Deflection at *C* [mm]	Error [%]	Comp. strain at *C* [mm/m]	Error [%]	Tens. strain at *C* [mm/m]	Error [%]	Comp. strain at *Q* [mm/m]	Error [%]
EXP PVB	9.84	–	-0.60	–	0.59	–	-0.44	–
FEM PVB_A	12.09	+22.89	-0.65	+8.32	0.65	+10.63	-0.49	+11.62
FEM PVB_B	11.22	+14.08	-0.62	+3.95	0.62	+6.16	-0.47	+7.22
FEM PVB_D	9.66	-1.80	-0.57	-3.94	0.57	-1.89	-0.43	-0.73
FEM PVB_H	13.51	+37.31	-0.69	+15.48	0.69	+17.94	-0.52	+18.83
FEM PVB_S	9.33	-5.21	-0.56	-5.63	0.56	-3.62	-0.43	-2.43
EXP EVA	12.44	–	-0.88	–	0.87	–	-0.66	–
FEM EVA_E	12.43	-0.12	-0.86	-1.50	0.86	-0.53	-0.65	-0.66

Table 2 summarizes the measured and predicted values and their errors for the largest loading pressure (before the collapse). Three sets of parameters, (Duser et al. 1999), (Shitanoki et al. 2014), and (Eitner 2011), provide the numerical prediction of the corresponding measured quantities with errors less than about 5%. The other three overestimated the response of laminated glass samples. The errors increased up to 37% for the data in (Hooper et al. 2012). The remaining two series in (Andreozzi et al. 2014) and (Biolzi et al. 2014) are more suitable for predictions of the long-term response; recall Figure 1.

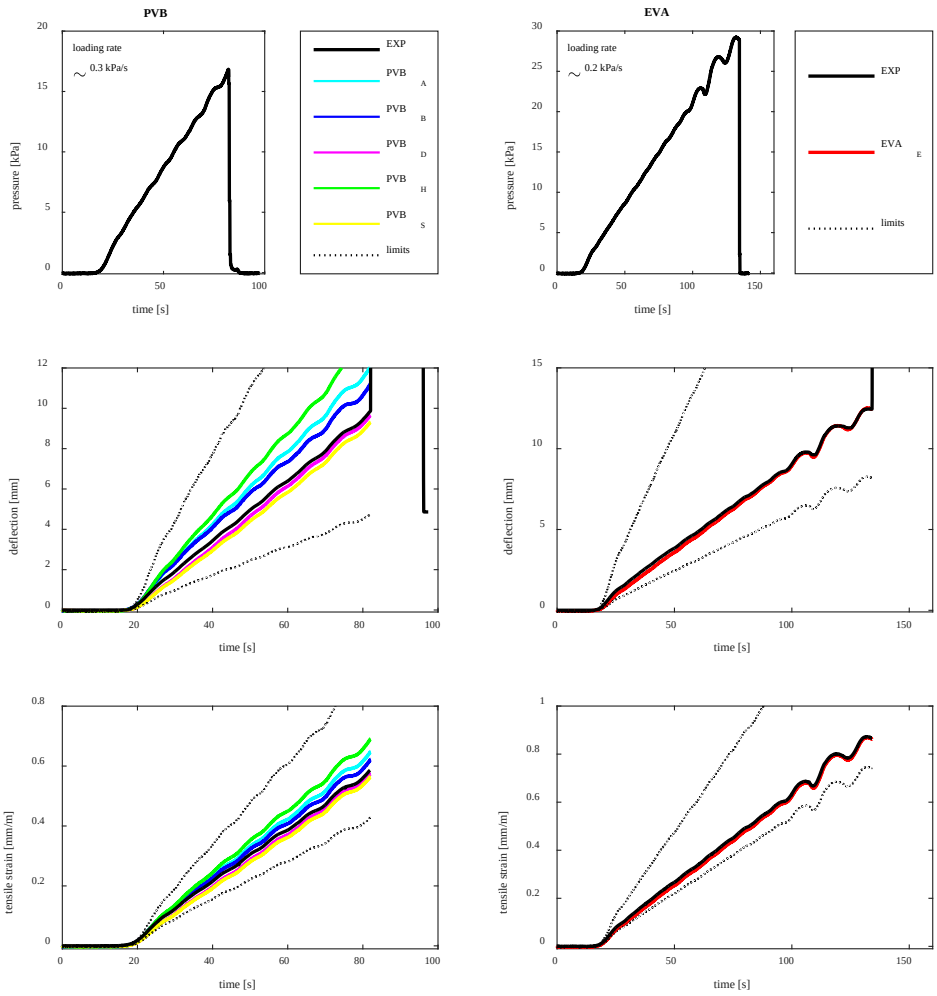

Fig. 5 Evolution of loading pressure, maximum deflection, and the largest value of tensile strain at the center for PVB and EVA samples.

5.2. Natural frequencies and modal loss factors from free vibration analysis

The experimental setup for modal analysis of laminated glass samples was introduced in Section 3.2. The numerical predictions, in terms of natural frequencies and loss factors, are shown in Table 3 and 4. The results were obtained by the complex-valued eigensolver from Section 4.2 and the material data for interlayers referenced in Table 1.

Table 3: Modal analysis: Comparison of experimental data and numerical predictions of natural frequencies for the first three mode shapes (MS).

Data	Natural frequency 1. MS [Hz]	Error [%]	Natural frequency 2. MS [Hz]	Error [%]	Natural frequency 3. MS [Hz]	Error [%]
EXP PVB	92.48	–	248.02	–	470.50	–
FEM PVB_A	70.92	-23.32	155.52	-37.30	281.26	-40.22
FEM PVB_B	63.42	-31.42	144.29	-41.82	268.46	-42.94
FEM PVB_D	96.90	+4.77	258.15	+4.08	491.43	+4.45
FEM PVB_H	95.28	+3.02	252.95	+1.99	477.48	+1.48
FEM PVB_S	97.24	+5.14	260.68	+5.11	493.95	+4.98
EXP EVA	81.08	–	183.76	–	320.31	–
FEM EVA_E	86.24	+6.37	196.15	+6.74	338.88	+5.80

The numerical prediction using series from (Duser et al. 1999), (Hooper et al. 2012), or (Shitanoki et al. 2014) provide the first three natural frequencies with the errors less than 5%; for the series from (Eitner 2011) below 7%. The other two series were adjusted for a lower frequency range, (Andreozzi et al. 2014), or for a long-term response, (Biolzi et al. 2014), and therefore the natural frequencies are underestimated by 20–45%.

Table 4: Modal analysis: Comparison of experimental data and numerical predictions of loss factors for the first three mode shapes (MS).

Data	Loss factor 1. MS [%]	Error [%]	Loss factor 2. MS [%]	Error [%]	Loss factor 3. MS [%]	Error [%]
EXP PVB	2.54	–	5.29	–	7.32	–
FEM PVB_A	0.08	-96.98	0.03	-99.47	0.01	-99.86
FEM PVB_B	0.00	-100.00	0.00	-100.00	0.00	-100.00
FEM PVB_D	1.01	-60.34	4.13	-22.06	7.72	+5.50
FEM PVB_H	4.93	+94.19	10.89	+105.60	12.21	+66.94
FEM PVB_S	0.95	-62.41	2.38	-55.12	3.74	-48.88
EXP EVA	2.57	–	4.50	–	4.44	–
FEM EVA_E	1.42	-44.71	2.48	-44.99	2.32	-47.77

Table 4 shows that all methods provide only an informative estimate of damping. The best agreement was found for the PVB sample with the parameters from (Duser et al. 1999). The error in loss factors are 60%, 22%, and 6% for the first, second, and third mode shape respectively. This discrepancy can be caused by the oscillatory character of the shear moduli plotted against the angular frequency; recall Figure 1. Increasing the number of viscoelastic units in the chain could improve the agreement with the experimental data.

6. Conclusions

The aim of this study was to assess the effect of mechanical properties of interlayers on the response of laminated glass elements. Six sets of parameters corresponding to the generalized Maxwell model (five for PolyVinyl Butyral and one for Ethylene-Vinyl Acetate) were selected from the literature, and their ability to accurately describe the behavior of tested laminated glass samples was examined for two examples.

For both the quasi-static and modal analysis, we compared the predictions of the numerical models using the different data from the literature with the experimental data. The results of this study are summarized in Figure 6. Each plot shows the errors of the numerical predictions of the tested quantities against the corresponding experimentally measured values. It can be seen that:

- The level of modal damping is highly sensitive to the material properties of the interlayer, and therefore, the errors in the modal loss factors are high for all used series. In most cases, the values of the loss factors are underestimated.
- Surprisingly, the best agreement with the experiment for the tested sample with the PolyVinyl Buthyral Trosifol BG R20 was found for the numerical prediction using the data for Butacite (Duser et al. 1999). The errors in the quasi-static response predictions and also in the natural frequencies were below 5%. However, the errors in loss factors increased up to 60%.
- The parameters for EthylenVinyl Acetate Etimex Vistasolar 496.10 (Eitner 2011) can be used to predict the quasi-static response of the tested sample with EthylenVinyl Acetate Evalam. In modal analysis, the natural frequencies were predicted with the errors below 7% and the loss factors below 50%.
- Nevertheless, one has to be careful dealing with data from the literature even for the same type of the interlayer foil.

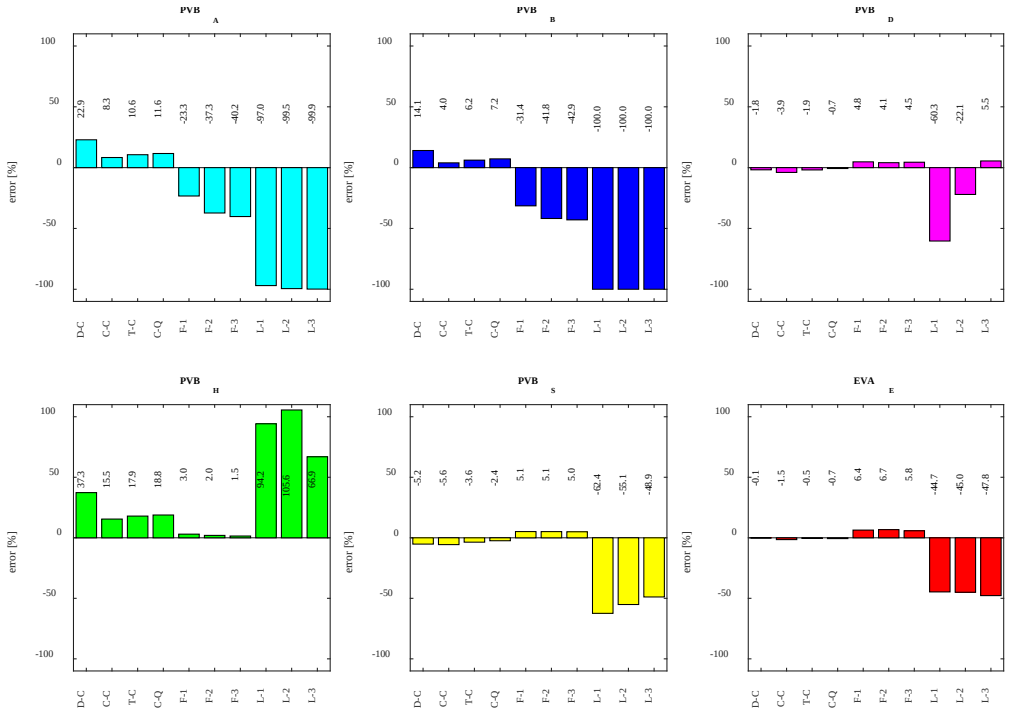

Fig. 6 Summary of errors for all tested quantities and all interlayers. (D-C deflection at the center, C-C compressive strain at the center, T-C tensile strain at the center, C-Q compressive strain at the quarter, F-1,2,3 natural frequency for the first, second, or third mode shape, L-1,2,3 loss factor for the first, second, or third mode shape).

For the reliable design of laminated glass structures and their analysis, the knowledge of mechanical properties of interlayers is essential. These conclusions demonstrate that the numerical models using the Maxwell chains parameters from the literature (for the same type of material) can provide unrealistic results. Reasons for the errors can be the difference in the content of additives depending on the manufacturer, or that the parameters of the generalized Maxwell model are used outside of the specific range of time/frequency domains, for which the chain was calibrated. This suggests the need for running, at least for a specific manufacturer, an independent experimental program and model calibration procedure to arrive at accurate and reliable predictions particularly in cases, where the viscoelastic properties of the polymer interlayer are decisive (Janda et al. 2016) or (Schmidt et al. 2017).

Acknowledgements

This publication was supported by the Czech Science Foundation under project No. 16-14770S. We would also like to thank Martina Eliášová, Tomáš Hána, Vladimír Hrbek, and Tomáš Plachý from Czech Technical University in Prague, the Centre of Excellence Telč, and the science center AdMaS at Brno University of Technology for performing the experimental measurements reported in this study.

References

Andreozzi, L., Briccoli Bati, S., Fagone, M., Ranocchiai, G., Zulli, F.: Dynamic torsion tests to characterize the thermo-viscoelastic properties of polymeric interlayers for laminated glass. Constr. Build. Mater. 65, 1–13 (2014). doi:10.1016/j.conbuildmat.2014.04.003

Biolzi, L., Cagnacci, E., Orlando, M., Piscitelli, L., Rosati, G.: Long term response of glass–PVB double-lap joints. Compos. Part B Eng. 63, 41–49 (2014). doi:10.1016/j.compositesb.2014.03.016

Christensen, R.M.: Theory of Viscoelasticity. Academic Press (2013)

Duser, A., Jagota, A., Bennison, S.: Analysis of Glass/Polyvinyl Butyral Laminates Subjected to Uniform Pressure. J. Eng. Mech. 125, 435–442 (1999). doi:10.1061/(ASCE)0733-9399(1999)125:4(435)

Eitner, U.: Thermomechanics of photovoltaic modules. Centre for Engineering Sciences, Martin Luther University of Halle-Wittenberg (2011)

Foraboschi, P.: Behavior and Failure Strength of Laminated Glass Beams. J. Eng. Mech. 133, 1290–1301 (2007). doi:10.1061/(ASCE)0733-9399(2007)133:12(1290)

Foraboschi, P.: Analytical model for laminated-glass plate. Compos. Part B Eng. 43, 2094–2106 (2012). doi:10.1016/j.compositesb.2012.03.010

Hooper, P.A., Blackman, B.R.K., Dear, J.P.: The mechanical behaviour of poly(vinyl butyral) at different strain magnitudes and strain rates. J. Mater. Sci. 47, 3564–3576 (2012). doi:10.1007/s10853-011-6202-4

Janda, T., Zemanová, A., Zeman, J., Šejnoha, M.: Finite element models for laminated glass units with viscoelastic interlayer for dynamic analysis. In: High Performance and Optimum Design of Structures and Materials II, WIT Transactions on The Built Environment. pp. 245–254. WIT Press, Southampton, UK (2016)

Larcher, M., Solomos, G., Casadei, F., Gebbeken, N.: Experimental and numerical investigations of laminated glass subjected to blast loading. Int. J. Impact Eng. 39, 42–50 (2012). doi:10.1016/j.ijimpeng.2011.09.006

Melcher, J., Karmazínová, M.: Experimentální verifikace procesu přetváření a únosnosti plošných dílců s využitím metody zatěžování vakuováním, Z/B – Ověřená technologie, RIV/00216305:26110/09:PR24352, in Czech, (2009)

Mohagheghian, I., Wang, Y., Jiang, L., Zhang, X., Guo, X., Yan, Y., Kinloch, A.J., Dear, J.P.: Quasi-static bending and low velocity impact performance of monolithic and laminated glass windows employing chemically strengthened glass. Eur. J. Mech. - ASolids. 63, 165–186 (2017). doi:10.1016/j.euromechsol.2017.01.006

Renaud, F., Dion, J.-L., Chevallier, G., Tawfiq, I., Lemaire, R.: A new identification method of viscoelastic behavior: Application to the generalized Maxwell model. Mech. Syst. Signal Process. 25, 991–1010 (2011). doi:10.1016/j.ymssp.2010.09.002

Schmidt, J., Janda, T., Šejnoha, M.: Experimental determination of visco-elasic properties of laminated glass interlayer. In: Engineering Mechanics 2017 - Book of full texts. Institute of Solid Mechanics, Mechatronics and Biomechanics, Brno (2017)

Shitanoki, Y., Bennison, S.J., Koike, Y.: A practical, nondestructive method to determine the shear relaxation modulus behavior of polymeric interlayers for laminated glass. Polym. Test. 37, 59–67 (2014). doi:10.1016/j.polymertesting.2014.04.011

Timmel, M., Kolling, S., Osterrieder, P., Du Bois, P.A.: A finite element model for impact simulation with laminated glass. Int. J. Impact Eng. 34, 1465–1478 (2007). doi:10.1016/j.ijimpeng.2006.07.008

Williams, M.L., Landel, R.F., Ferry, J.D.: The temperature dependence of relaxation mechanisms in amorphous polymers and other glass-forming liquids. J. Am. Chem. Soc. 77, 3701–3707 (1955)

Zemanová, A., Zeman, J., Janda, T., Schmidt, J., Šejnoha, M.: On modal analysis of laminated glass: Usability of simplified methods and enhanced effective thickness. arXiv:1801.01110. (2018)

Zemanová, A., Zeman, J., Šejnoha, M.: Comparison of viscoelastic finite element models for laminated glass beams. Int. J. Mech. Sci. 131–132, 380–395 (2017). doi:10.1016/j.ijmecsci.2017.05.035